Astronomy in Focus - XXX
Proceedings IAU Symposium No. XXX, 2018
M. T. Lago, ed.

doi:10.1017/S174392131900512X

Gaia Photometric Catalogue: the calibration of the DR2 photometry

D. W. Evans[1], M. Riello[1], F. De Angeli[1], J. M. Carrasco[2], P. Montegriffo[3], C. Fabricius[2], C. Jordi[2], L. Palaversa[1], C. Diener[1], G. Busso[1], C. Cacciari[3], E. Pancino[4] and F. van Leeuwen[1]

[1]Institute of Astronomy, University of Cambridge, Madingley Road, Cambridge CB3 0HA, UK
[2]Institut de Ciències del Cosmos, Universitat de Barcelona (IEEC-UB), Martí Franquès 1, 08028 Barcelona, Spain
[3]INAF–Osservatorio Astronomico di Bologna, via Ranzani 1, 40127 Bologna, Italy
[4]INAF - Osservatorio Astronofisico di Arcetri, Largo Enrico Fermi 5, 50125, Firenze, Italy
email: dwe@ast.cam.ac.uk

Abstract. Gaia DR2 was released in April 2018 and contains a photometric catalogue of more than 1 billion sources. This release contains colour information in the form of integrated BP and RP photometry in addition to the latest G-band photometry. The level of uncertainty can be as good as 2 mmag with some residual systematics at the 10 mmag level. The addition of colour information greatly enhances the value of the photometric data for the scientific community. A high level overview of the photometric processing, with a focus on the improvements with respect to Gaia DR1, was given. The definition of the Gaia photometric system, a crucial part of the calibration of the photometry, was also explained. Finally, some of the photometric improvements expected for the next data release were described.

Keywords. Catalogues, Surveys, Techniques: photometric

1. Introduction

The release of Gaia DR2 (Gaia Collaboration 2018) was a big step up from Gaia DR1 not only for the astrometry, but also the photometry in that colours for more than 1.3 billion sources were released. The presentation given described the processing and calibrations that went into generating the photometric data. See Evans *et al.* (2018) and Riello *et al.* (2018) for more details.

2. Internal calibrations

It is important to remember that the photometry in the different bands originates from two different sources on-board the satellite as this explains the different systematics. The G-band fluxes are the result of a fit to a set of corrected samples or pixels from the Astrometric Field (AF) CCDs. This fit consists of a Line or Point Spread Function (LSF/PSF) depending on whether the data is 1D or 2D. Only the brighter sources have 2D data transmitted to the ground for reasons of bandwidth limitation. The samples or pixels are corrected for bias and various background components e.g. charge release, straylight. These corrections are described in Hambly *et al.* (2018). The colour photometry comes from the prism-dispersed spectra on the BP (blue) and RP (red) CCDs. The photometric measurements are the results of summing up the bias and background-corrected samples and are equivalent to aperture photometry.

The basic principle of the calibration is one of a detailed iterative self-calibration followed by an external calibration which determines the zeropoints and the passbands

that best represent the internal reference system (Carrasco *et al.* 2016). Since there is no photometric catalogue suitable for calibrating the Gaia photometry in detail, i.e. deep enough, all-sky, in the same photometric system and accurate at the mmag level, the main photometric calibration has to be carried out using the Gaia data itself. The task therefore is to calibrate the raw data onto a photometric system that represents the average instrument. By doing this, we ensure that a large number of sources can be used even for the rarest configurations of the satellite.

The general scheme of the iterative internal calibration is shown in Figure 1. The initial stage is to use all the raw photometric data for a source to form a crude average. Data is excluded from the periods of bad contamination for this initialization process. These averages are then used as reference values for calibrations which are calculated separately for each CCD, field-of-view and different configuration (gate and window class). The model for these calibrations includes the coordinate across the CCD and detailed colour information. The time variation is accounted for by calculating these calibrations per day of the mission. Following this initial calibration, calibrated photometry is used to form a new set of average fluxes for each source which then serve as reference fluxes to generate a new set of calibrations. This scheme is then iterated. A further set of calibrations gets carried out after this iterative scheme to account for a more detailed variation in response across each CCD. This is equivalent to a 1D flat field which is appropriate since the CCDs are read out in time-delayed integration mode.

The iterative scheme described here only works if the majority of sources are observed under many different conditions and the different observing configurations include many sources. In general, this is the case, but for the cases when this is a problem, special link calibrations are carried out. See Riello *et al.* (2018) for more details on these. Note that since this iterative initialization of the reference system is carried out for each processing cycle (which ends in a data release) and the data used for the initialization is different in the two cycles, the photometric system for DR2 is not the same as that for DR1.

Unexpected complexities have affected the photometric calibrations which were the result of unforeseen satellite problems. Soon after the mission started, it was seen that the photometric throughput was degrading at a rate higher than expected. This was caused by water from the spacecraft depositing as ice layers on the mirrors and the CCDs. This has been mitigated by periodically heating the mirrors and CCDs to remove this contaminant. During the period of the main mission, this decontamination procedure has been carried out three times. A consequence of this variation in throughput (by up to 0.5 mag) is to stress the photometric initialization process and to affect the detection limit at certain points of the mission. Another problem was one of additional straylight adding to the background level of the observations. This was caused by sunlight being scattered into the optical path by untrimmed fibres on the edge of the sunshield. This meant that the background-subtraction algorithms had to be improved to handle the large and rapid variations of this straylight component. However, at the faint end, there is a loss of performance and the G-band photometry is now sky limited. See Gaia Collaboration (2016) for more details about the satellite and the issues that affected the data.

3. Validation and testing

The precision of the G-band photometry is shown in Figure 2. This analysis is restricted to sources with about 100 CCD observations. By doing this, it is possible to compare the performance with nominal expectations. This nominal expected precision can also be convolved with a calibration floor to get an idea of the size of the uncalibrated effects that remain in the data at the individual CCD measurement level. For the G-band this is 2 mmag. At the bright end, the deviation from nominal is probably caused by saturation effects and problematic calibrations that have too few calibrators. The bumps at G=13

https://doi.org/10.1017/S174392131900512X Published online by Cambridge University Press

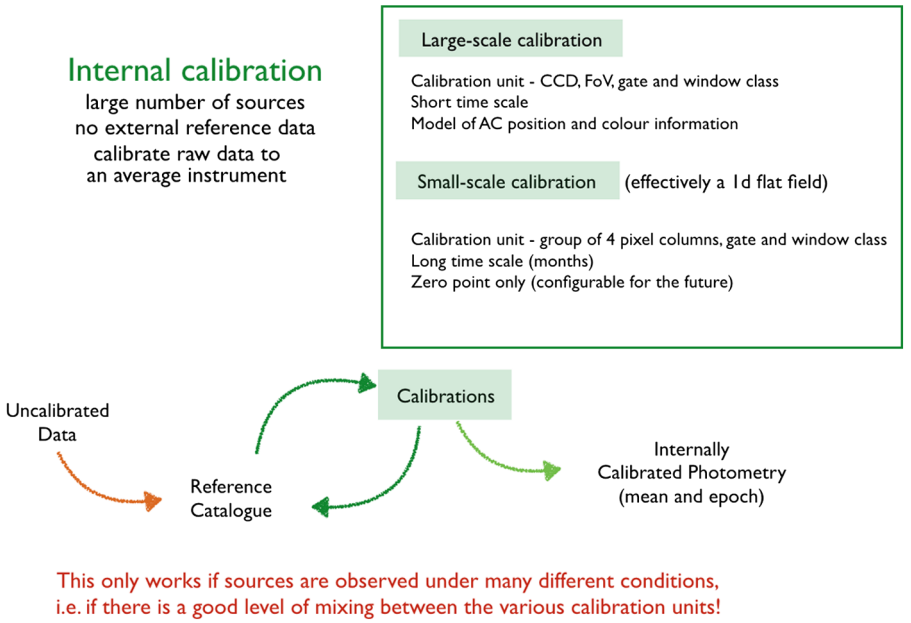

Figure 1. The general principle of the iterative internal calibration.

and 16 are linked to changes in the windowing configuration and some photometric inhomogeneities. At the faint end, it can be seen that the performance is poorer than expected due to the higher levels of straylight encountered in comparison to expectation. Whereas the expectation at the faint end of the G-band performance was that the observations would be source dominated, they are now sky dominated.

By restricting the analysis to sources with a fixed number of observations, a comparison between DR1 and DR2 was also possible and it shows that the performance has improved across the whole magnitude range.

Results were also shown for the BP and RP performances which had far fewer features in the uncertainty distribution than the G-band. This is due to fewer configuration changes and less saturation effects being present and to the overall larger uncertainties. The calibration floor for these passbands are 5 and 3 mmag for BP and RP respectively.

External catalogue comparisons have also been made, but suffer from the uncertainty in the source of any differences observed. In some cases it is clear that the difference has a Gaia origin due to the magnitude this occurs at corresponding to a Gaia configuration change. At G=13 and 16, small discontinuities remain at the 2–3 mmag level which is significantly smaller than those seen in the DR1 photometry. These comparisons also show possible background issues at the faint end.

Internal consistency checks can also be made between the three passbands. However, if differences are seen here, it is difficult to identify in which passband the features originate. An example of this can be seen in Figure 31 of Arenou *et al.* (2018). This shows a magnitude trend for sources brighter than G = 16 which is likely to be present in the G-band. This has been identified in a number of papers (Weiler 2018, Maíz Apellániz & Weiler 2018 and Casagrande & VandenBerg 2018). The likely cause of this magnitude trend is in the LSF/PSF fitting which generates the G-band fluxes where a non-time-varying calibration was used for the LSF/PSFs. Fainter than G = 16, the origin of the "hockey stick" feature seen can not be determined since it is likely that background issues are present in all three passbands.

https://doi.org/10.1017/S174392131900512X Published online by Cambridge University Press

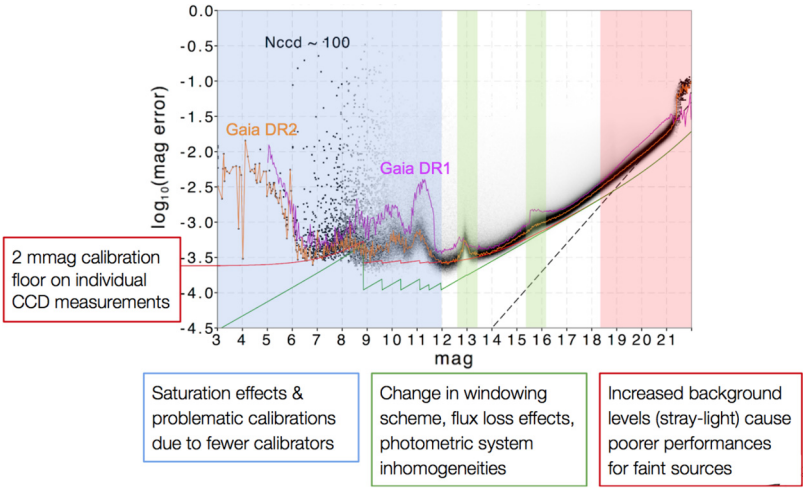

Figure 2. Precision of the G-band photometry. This analysis is restricted to sources with about 100 CCD observations. This enables a comparison to be made with nominal expectations (green line) and also facilitates the comparison between DR1 (magenta) and DR2 (orange). The red line is as the green one, but convolved with a 2 mmag calibration floor. The black dotted line has a gradient of 0.4 and shows the faint end to be sky dominated.

4. External calibration and the passbands

In addition to the G, BP and RP photometry, DR2 also released passbands that best represented the internal photometric system. These passbands were determined solely from the spectrophotometric data gathered for this specific determination. The version of this data used was SPSS V1. See Pancino *et al.* (2012) for more details on the SPSS catalogue.

Since the publication of DR2, two sets of alternative passbands have been published. Of these, the ones in Maíz Apellániz & Weiler (2018) are probably the best to use although note that there is no physical reason for the 2 passbands given for BP. The effects leading to this is likely to be a consequence of the photometric system not converging properly for sources with BP−RP<0.0. The main reason that these passbands are probably better than those released with DR2 is that additional information was used to help with the behaviour for very red sources, where the SPSS is lacking in data. Note that if you use these passbands, you must also use the zeropoints and G-band magnitude terms as formulated by the same authors. It is also important not to extrapolate the G-band magnitude terms fainter than G = 16 since the linear model used is not appropriate there and no comparison data was available.

An important point to consider is whether the magnitude term in the G-band determined in these papers is valid or not i.e. if the CALSPEC (Bohlin *et al.* 2017) magnitude scale is accurate at the mmag level. The clearest evidence for this comes from Figure 1 of Casagrande & VandenBerg (2018). At the very least, this shows that the BP and RP photometry are on the same magnitude scale as that of CALSPEC.

A final note of warning regarding the use of Gaia passbands in general. Even though much work has been done in building up a set of spectrophotometric standards, both SPSS and CALSPEC, they are not numerous, especially at the red end. The consequence of this is that the passbands are weakly constrained by this spectrophotometric data and that better results can be achieved by cross-matching photometric datasets with DR2 to derive colour-colour relationships.

https://doi.org/10.1017/S174392131900512X Published online by Cambridge University Press

5. The next data release

The next data release for Gaia is now scheduled for the first half of 2021. This release will contain a new data type which will be the internally calibrated mean source spectra. These are the prism-dispersed spectra that are gathered on the BP and RP CCDs. The external calibration of these spectra will be in the form of a utility that can convert a user-supplied SED into the system and resolution of the Gaia internally calibrated spectra.

Additionally, the photometry will be improved with respect to the DR2 performances. The LSF and PSF calibrations will be more sophisticated resulting in improved G-band photometry which should reduce any magnitude trends. Better background subtraction algorithms will also be used for both the G-band and for BP/RP. The robustness of the averaging algorithm used to compute the mean source photometry will be improved resulting in fewer sources with significantly incorrect magnitudes. Also, a more sophisticated processing of the BP/RP spectra in crowded regions will be used.

Acknowledgments

This work has made use of data from the European Space Agency (ESA) mission *Gaia* (https://www.cosmos.esa.int/gaia), processed by the *Gaia* Data Processing and Analysis Consortium (DPAC, https://www.cosmos.esa.int/web/gaia/dpac/consortium). Funding for the DPAC has been provided by national institutions, in particular the institutions participating in the *Gaia* Multilateral Agreement.

References

Arenou, F., Luri, X., Babusiaux, C. *et al.* 2018, *A&A* 616, A17
Bohlin, R. C., Mészáros, S., Fleming, S. W., *et al.* 2017, *AJ* 153, 234
Carrasco, J. M., Evans, D. W., Montegriffo, P. *et al.* 2016, *A&A* 595, A7
Casagrande, L., & VandenBerg, D.A. 2018, *MNRAS* 479, L102
Evans, D. W., Riello, M., De Angeli, F. *et al.* 2018, *A&A* 616, A4
Gaia Collaboration (Prusti, T., *et al.*) 2016, *A&A* 595, A1
Gaia Collaboration (Brown, A. G. A., *et al.*) 2018, *A&A* 616, A1
Hambly, N., Cropper, M., Boudreault, S., *et al.* 2018, *A&A* 616, A15
Maíz Apellániz, J. & Weiler, M. 2018, arXiv:1808.02820
Pancino, E., Altavilla, G., Marinoni, S., *et al.* 2012 *MNRAS* 426, 1767
Riello, M., De Angeli, F., Evans, D. W., *et al.* 2018, *A&A* 616, A3
Weiler, M. 2018, *A&A* 617, A138